Dalton Transactions

An international journal of inorganic chemistry

rsc.li/dalton

ROYAL SOCIETY
OF CHEMISTRY
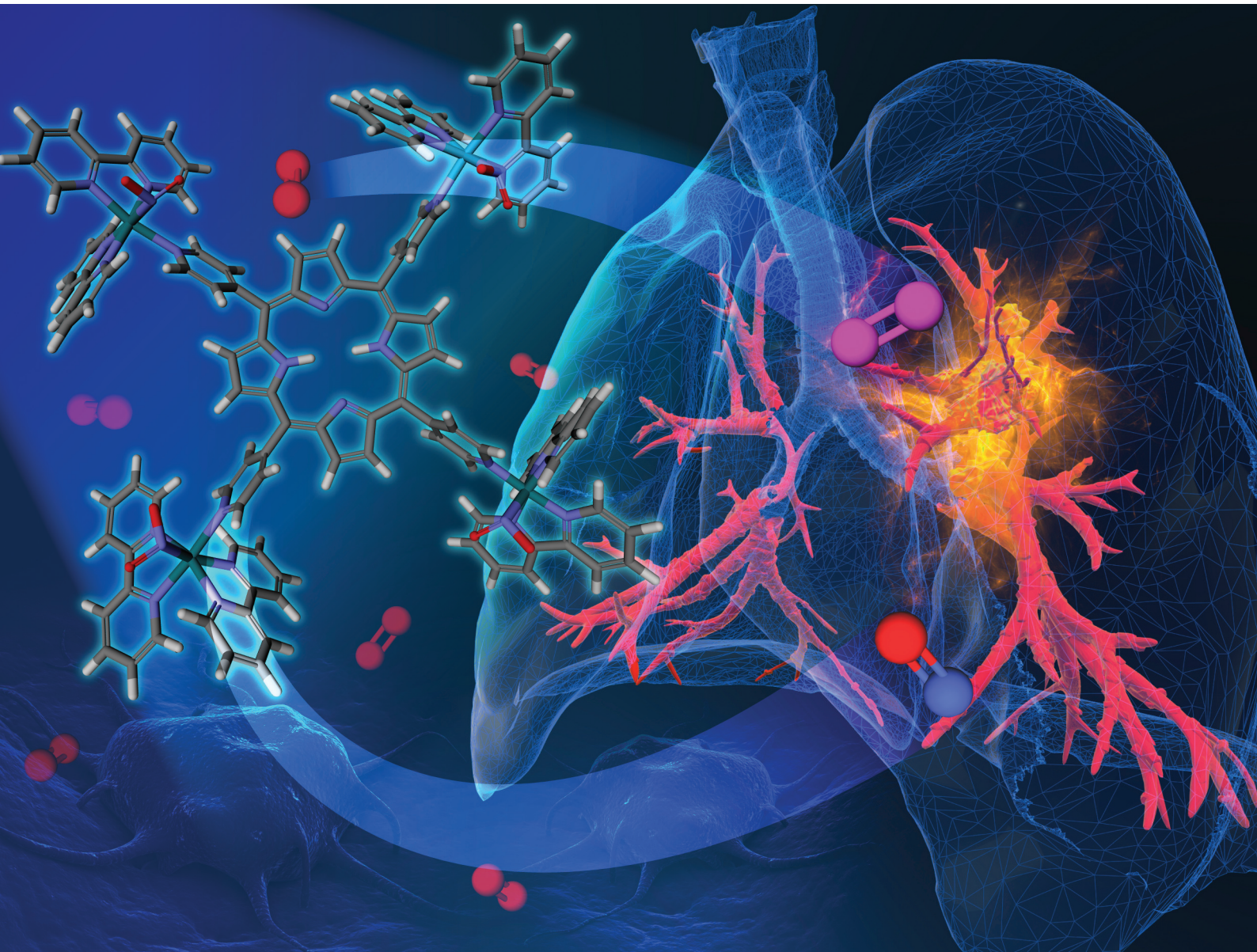
PAPER
Roberto Santana da Silva *et al.*
The effect of light irradiation on a nitro-ruthenium porphyrin complex in the induced death of lung cancer cells in two- and three-dimensional cultures: Insights into the effect of nitric oxide

Dalton Transactions

PAPER

Check for updates

The effect of light irradiation on a nitro-ruthenium porphyrin complex in the induced death of lung cancer cells in two- and three-dimensional cultures: Insights into the effect of nitric oxide†

Amanda Blanque Becceneri,*[a] Matheus Torelli Martin,[a]
Angelica Ellen Graminha, [ID][a,b] Márcia Regina Cominetti, [ID][c] Peter C. Ford [ID][d] and
Roberto Santana da Silva [ID][a,d]

Efforts to find compounds selectively affecting cancer cells while sparing normal ones have continued to grow. Nitric oxide (NO) is critical in physiology and pathology, including cancer. It influences cellular processes like proliferation, apoptosis, and angiogenesis. The intricate interaction of NO with cancer cells offers innovative treatment possibilities, but its effects can vary by concentration and site. Ruthenium complexes capable of releasing NO upon stimulation show for this purpose. These versatile compounds can also enhance photodynamic therapy (PDT), a light-activated approach, which induces cellular damage. Ruthenium-based photosensitizers (PSs), delivering NO and producing reactive oxygen species (ROS), offer a novel strategy for improved cancer treatments. In this study, a nitro-ruthenium porphyrin conjugate: $\{TPyP[Ru(NO_2)(bpy)_2]_4\}(PF_6)_4$, designated $RuNO_2TPyP$, which releases NO upon irradiation, was investigated for its effects on lung cells (non-tumor MRC-5 and tumor A549) in 2D and 3D cell cultures. The findings suggest that this complex has potential for PDT treatment in lung cancer, as it exhibits photocytotoxicity at low concentrations without causing cytotoxicity to normal lung cells. Moreover, treatment of cells with $RuNO_2TPyP$ followed by light irradiation (4 J cm^{-2}) can induce apoptosis, generate ROS, promote intracellular NO formation, and has anti-migratory effects. Additionally, the complex can modify tumor cell structures and induce photocytotoxicity and apoptosis in a 3D culture. These outcomes are attributed to the internalization of the complex and its subsequent activation upon light irradiation, resulting in NO release and singlet oxygen production.

1 Introduction

In recent years, significant endeavors have been directed toward discovering compounds capable of selectively affecting cancer cells.[1–4] Compounds that leverage inherent metabolic disparities between these cell types, as is evident from the ability of tumor cells to modify their metabolism and regulate cell proliferation and growth, will have the potential to offer more potent treatments. This approach could lead to the reduction of adverse effects on patients by precisely targeting tumor cells.[5,6] Some studies in this direction have highlighted the role of neurotransmitters as chemical mediators capable of activating specific receptors that influence the growth of cancer cells.[7]

Given this context, significant focus has been directed towards nitric oxide (NO), an innate molecule that assumes a multitude of intricate roles in a broad spectrum of physiological and pathological processes, notably within vascular function. The significance of NO extends to its capacity for governing diverse cellular mechanisms such as proliferation, apoptosis, angiogenesis, and cancer progression. This interplay between neurotransmitters like NO and the conduct of cancer cells underscores the potential for pioneering therapeutic approaches that could harness these signaling pathways to enhance cancer treatment outcomes. Nevertheless, the multifaceted nature of NO leads to ongoing debates, and its impact

*[a]Laboratory of Photochemistry and Bioinorganic Chemistry,
School of Pharmaceutical Sciences of Ribeirão Preto, University of São Paulo (USP),
Av. do Café, Vila Monte Alegre, Ribeirão Preto, São Paulo, 14040-903, Brazil.
E-mail: amandabecc@usp.br*
*[b]Institute of Chemistry, São Paulo State University, Av. Prof. Francisco Degni, 55,
14800-900, Araraquara, São Paulo, Brazil*
*[c]Department of Gerontology, Federal University of São Carlos, Rod. Washington Luís,
Km 235, São Carlos, São Paulo, 13565-905, Brazil*
*[d]Department of Chemistry and Biochemistry, University of California, Santa Barbara,
California 93110-9510, USA*
†Electronic supplementary information (ESI) available. See DOI: https://doi.org/
10.1039/d4dt00381k

appears contingent on concentration and specific location. At higher concentrations, NO has demonstrated cytotoxic effects.[8,9]

Among various NO-donating agents, ruthenium complexes have gained attention for their capacity to deliver appropriate NO levels upon stimulation.[10–12] These versatile ruthenium multi-function compounds can potentially contribute significantly to non-traditional cancer treatment modalities such as photodynamic therapy (PDT). PDT is a minimally invasive therapeutic modality that operates on the intricate interplay of three essential components: a photosensitizer (PS), a light source with an appropriate wavelength to activate the PS, and molecular oxygen. The mechanism underlying PDT entails photochemical and photophysical processes triggered by the absorption of light by the PS. Within this process, the PS can transfer energy or electrons, generating reactive species, such as singlet oxygen and hydroxyl radicals, which play crucial roles in initiating cellular damage, ultimately resulting in cellular death through apoptosis, necrosis, or other forms of cell death.[13–15] To ensure the effectiveness of PDT, the PSs should have specific characteristics, including the absence of dark toxicity, to minimize harm to normal tissues before light activation.[16]

The use of transition metal complexes as PSs holds great promise as another cancer treatment.[17] Notably, transition metals can be effectively combined with porphyrins, known for their unique electronic structure and spectroscopic characteristics.[18,19] This synergistic combination facilitates the development of metal-based PSs that enhances the catalytic properties of porphyrins. The most promising metal-based PSs developed for clinical use include tetrapyrrolic derivatives based on porphyrin or Pd(II) chlorins (WST11 for prostate cancer), Lu(III) (Lutes, lutetium texaphyrin for cervical cancer), Sn(IV) (Purlytin, macular degeneration), and ruthenium-based derivatives.[20–23] Therefore, the ability of ruthenium complexes to donate NO upon irradiation and to enhance photocatalytic properties of the PS in the production of reactive oxygen species (ROS) can be a promising strategy.

In a previous study, we synthesized and evaluated a new porphyrin complex, designated as RuNO$_2$TPyP, with the molecular formula $C_{120}H_{90}F_{24}N_{28}O_8P_4Ru_4$. This complex features nitro-ruthenium groups coordinated by pyridyl bridges, specifically {TPyP[Ru(NO$_2$)(bpy)$_2$]$_4$}(PF$_6$)$_4$, where TPyP stands for 5,10,15,20-tetra(4-pyridyl)porphyrin and bpy represents 2,2′-bipyridine. The absorption spectrum of this complex revealed a distinct Soret band at 421 nm, which is characteristic of porphyrin compounds. Moreover, this complex demonstrated significant photocytotoxicity in melanoma tumor cells (B16–F10), as it produced singlet oxygen (Φ_Δ = 0.29) and released NO (Φ_{NO} = 2.63 × 10^{-5}) upon irradiation at 415 nm.[24] Based on previous findings, further investigations were carried out to assess the *in vitro* potential of RuNO$_2$TPyP. The present study investigates the effects of the complex on lung cancer A549 cells and non-tumor cell line MRC-5 in 2D and 3D cell cultures.

2 Materials and methods

2.1 Cells

The lung cell lines used were MRC-5 (human non-tumor lung cells) and A549 (human non-small cell lung cancer). The cells were maintained in Dulbecco's modified Eagle's medium (DMEM) containing 10% of fetal bovine serum (FBS), L-glutamine (2 mM), penicillin (100 IU mL^{-1}) and streptomycin (100 mg mL^{-1}) and incubated at 37 °C with 5% CO$_2$ in a humidified incubator.

2.2 Ruthenium complex

RuNO$_2$TPyP was synthesized and characterized using methods given in our previously published study.[24] The structure of the complex is shown in Fig. 1. Details regarding its characterization, including ^{1}H-NMR spectroscopy and mass spectrometry data, are also provided in the earlier study. To further clarify, mass spectrometry spectra are presented in Fig. S1 of the ESI.† The complex was solubilized in 100% dimethyl sulfoxide (DMSO), and the maximum concentration of DMSO used for cell treatment was 1%.

2.3 Light source

The light source used for irradiation assays involved in PDT experiments consisted of LED arrays (Elétron Comercial, Brazil) with a wavelength of 415 nm and an irradiance of 0.06846 W cm^{-2}.

2.4 2D assays

2.4.1 Dark cytotoxicity and photocytotoxicity assay – MTT method. Initially, the cytotoxic effects of RuNO$_2$TPyP were
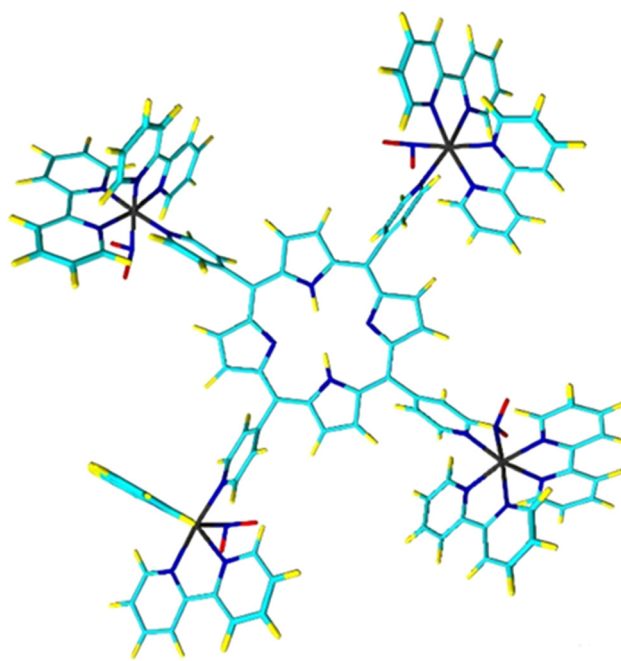

Fig. 1 Proposed molecular structure of the $C_{120}H_{90}F_{24}N_{28}O_8P_4Ru_4$ complex.

determined by the 3-(4,5-dimethylthiazol-2-yl)-2,5-diphenylte-trazolium bromide (MTT) cell viability assay, based on the methodology described previously.[25] Briefly, cells (1×10^4 cells per well) were plated onto 96-well plates and incubated at 37 °C and 5% CO_2 for 24 h. Afterward, the culture medium was removed, and different concentrations (0–50 µM) of the complex were added to the wells for a period of 4 h or 24 h. Next, the treatment was removed, and a fresh medium without phenol red was added. Then, one group of cells was irradiated at 415 nm (4 J cm^{-2}), while the other group was kept in the dark. Afterward, both groups of cells were incubated for an additional 20 h under same conditions, as mentioned earlier. Subsequently, the supernatant was removed, and MTT solution (0.5 mg mL^{-1}) was added for 3 h. Resulting formazan crystals were then solubilized in 100% DMSO. The results were analyzed using a microplate reader (BioTek Synergy HT, Agilent) at a wavelength of 540 nm. The viability of treated cells was normalized to that of negative control cells (without treatment). The IC$_{50}$ calculation was performed using GraphPad® Prism software, version 8.

2.4.2 Cellular uptake. The A549 cells were plated at a density of 1.5×10^6 cells in 10 cm Petri dishes and incubated for 24 h. Subsequently, the cells were treated with 0.5 µM of the RuNO$_2$TPyP and incubated for either 4 h or 24 h. Following incubation, the Petri dishes were washed twice with PBS, and the cells were collected using a cell scraper. Cell pellets were digested with pure nitric acid for 1.5 h at 60 °C. After digestion, samples were diluted appropriately with ultra-pure water to achieve a nitric acid concentration of 2% before using them for further analysis. The determination of total ruthenium content was performed using inductively coupled plasma mass spectrometry (ICP-MS) on a NexION 2000 instrument (PerkinElmer, Norwalk, CT, USA), operated with high-purity argon (99.99%, Air Liquide, Brazil). Analytical calibration standards were prepared using a 2% nitric acid solution with RuCl$_3$·3H$_2$O, purified by sub-boiling distillation using a quartz distiller (Kürner Analysentechnik, Rosenheim, Germany).

2.4.3 Cell morphology assay. To evaluate the effect of RuNO$_2$TPyP on the morphology of the A549 and MRC-5 cells, the cells were seeded (1×10^5 cells per well) onto 12-well plates and maintained at 37 °C and 5% CO_2 for 24 h. The following day, the complex at a concentration of 0.5 µM was added for 4 h, after the supernatant was removed, and a fresh medium without phenol red was added. The cells were then irradiated with a dose of 4 J cm^{-2} at 415 nm and incubated for 20 h at same conditions described above. Photographs were captured 24 h after treatment using a camera (Nikon DS-U3) attached to a Nikon Eclipse Ti microscope. The images were acquired with a 100× optical zoom.

2.4.4 Cell colony formation assay. For the analysis of the cytotoxic and cytostatic potential of RuNO$_2$TPyP, the A549 and MRC-5 cells (3×10^2 cells per well) were cultured onto 6-well plates and incubated at 37 °C and 5% CO_2 for 24 h. After this period, the complex (0.5 µM) was added for a 4 h period, after the supernatant was removed, and a fresh medium without

phenol red was added. The cells were then irradiated with a dose of 4 J cm^{-2} at 415 nm and incubated for an additional 10 d. After this period, the supernatant was discarded, and the cells were fixed with a solution of methanol and acetic acid in a 3 : 1 ratio and later stained with a solution of methanol and crystal violet (5%). Images were captured using a Chemidoc® photodocumenter (BioRad).

2.4.5 Cell migration assay – wound healing. To determine the effect of complex RuNO$_2$TPyP on cell migration, the A549 and MRC-5 cells (1×10^5 cells per well) were cultured onto sterile 12-well plates. These were maintained at 37 °C and 5% CO_2 until the culture reached a high confluence. Then, with a 200 µL pipette tip, a scratch was made in the center of each well. The wells were washed with PBS, and the cells were treated with the complex (0.06 µM) for 4 h. The treatment complex was removed, and a fresh medium without phenol red was added. Next, the cells were irradiated with a dose of 4 J cm^{-2} at 415 nm and incubated at the same conditions for 48 h. The images were acquired with a 100× optical zoom at 0 h (immediately after irradiation), and at 24 h and 48 h after irradiation. The area of closure of the scratch due to cell migration was measured using Image J software, and the closure percentage was calculated according to the formula described earlier.[26]

2.4.6 Apoptosis assay. To verify the effect of RuNO$_2$TPyP on apoptosis, a phycoerythrin (PE) Annexin V Apoptosis Detection kit (BD Biosciences) was used. Briefly, the A549 and MRC-5 cells were seeded (1×10^5 cells per well) onto sterile 12-well plates and incubated at 37 °C and 5% CO_2 for 24 h. Then, the cells were treated with RuNO$_2$TPyP (2 µM) for 4 h, and after the treatment complex was removed, a fresh medium without phenol red was added, and the cells were irradiated with a dose of 4 J cm^{-2} at 415 nm and incubated for 20 h at same conditions described above. After the irradiation period, the cells were collected with TrypLE Express reagent (Gibco), washed with PBS, and suspended in 200 µL of binding buffer containing 5 µL of 7-amino-actinomycin D (7AAD) and 5 µL of PE Annexin V for 15 min protected from light. After incubation, flow cytometry was performed using a Accuri C6 cytometer (BD), and data were analyzed with the BD CSampler program.

2.4.7 Cell cycle assay. To investigate the effect of RuNO$_2$TPyP on the cell cycle, the A549 and MRC-5 cell lines were seeded (5×10^5 cells per well) onto sterile 6-well plates and incubated at 37 °C and 5% CO_2 for 24 h. Subsequently, the cells were incubated with the complex (0.5 µM) for 4 h, after which the treatment was removed, and a fresh medium without phenol red was added. The cells were then irradiated with a dose of 4 J cm^{-2} at 415 nm and incubated for an additional 20 h. After this period, the cells were collected, washed with PBS, and resuspended in chilled ethanol (70%), and left for 24 h at −20 °C. Next, the supernatant was removed after centrifugation, and the cells were incubated in a solution containing RNase A (20 µg mL^{-1}) and propidium iodide (PI; 10 µg mL^{-1}) at 37 °C for 30 min. Flow cytometry analysis was performed on an Accuri C6 cytometer (BD), and the data were analyzed using the BD CSampler analysis software.

2.4.8 Interaction with albumin and transferrin assay. To evaluate the cellular interaction of RuNO$_2$TPyP with bovine serum albumin (BSA) and human transferrin (apo-Tf), the cells were seeded (1×10^4 cells per well) onto sterile 96-well plates and maintained at 37 °C in a humidified incubator with 5% CO$_2$ for 24 h. After incubation, the cells were treated with a fixed concentration of 0.25 μM of RuNO$_2$TPyP combined with different concentrations of BSA (75 and 300 μg mL^{-1}) and apo-Tf (25 and 50 μg mL^{-1}) for 4 h. After the treatment complex was removed, a fresh medium without phenol red was added. The cells were irradiated with a dose of 4 J cm^{-2} at 415 nm and left for further incubation for 20 h. As described earlier, the percentage of viable cells was determined using the MTT reagent.

2.4.9 NO induction assay. To evaluate the induction of NO generation by RuNO$_2$TPyP treatment followed by light irradiation, cells (1×10^5 cells per well) were cultured onto sterile 12-well plates at 37 °C and 5% CO$_2$ for 24 h. Subsequently, the cells were incubated with the complex for 4 h (0.5 μM), and after the treatment complex was removed, a fresh medium without phenol red was added. The cells were then irradiated with a dose of 4 J cm^{-2} at 415 nm and incubated for an additional 20 h. Next, they were washed with PBS and incubated with 5 μM of 4-amino-5-methylamino-2′,7′-difluorescein (DAF-FM) for 30 min at 37 °C. After incubation, the cells were rewashed with PBS, and a culture medium without phenol red was added for the fluorescence microscopy analysis (Nikon Eclipse Ti). The images were acquired with a 100× optical zoom.

2.4.10 Intracellular reactive oxygen species (ROS) level measured by DCFH-DA staining. The cells were initially seeded onto 24-well plates at a density of 0.5×10^5 cells per well and incubated at 37 °C with 5% CO$_2$ for 24 h. Subsequently, the cells were treated with the complex for 1.5 h at a concentration of 1 μM. Afterward, the treatment complex was removed, and a fresh medium without phenol red was added. The cells were then exposed to irradiation with a dose of 4 J cm^{-2} at 415 nm. Immediately following the irradiation, 50 μM of dichlorodihydrofluorescein diacetate (DCFH-DA) was added, and the cells were incubated at 37 °C for 40 min. Following this incubation period, the cells were washed twice with PBS and cultured in a phenol red free medium for subsequent fluorescence microscopy analysis using a Nikon Eclipse Ti microscope. The images were acquired with a 100× optical zoom. As a positive control, the cells were treated with hydrogen peroxide at a concentration of 10 000 μM for 1.5 h.

2.4.11 Phalloidin labeling assay. The effects of treatment with RuNO$_2$TPyP on the cytoskeleton of the A549 and MRC-5 cells after irradiation were verified using the Alexa Fluor® 488 Phalloidin antibody. The cells (1×10^4 cells per well) were plated onto 10-well sterile black plates and maintained at 37 °C in a humidified incubator with 5% CO$_2$ for 24 h. Next, the cells were treated with RuNO$_2$TPyP (0.25 μM) for 4 h, and then, the treatment complex was removed, and a fresh medium without phenol red was added. The cells were then irradiated with a dose of 4 J cm^{-2} at 415 nm and incubated for

20 h. The cells were washed with PBS and were then subjected to fixation in 4% paraformaldehyde in PBS for 20 min and further permeabilized with 0.1% Triton-X 100 in PBS for 5 min at room temperature. Subsequently, the plates were subjected to a 30 min blocking step with 2% BSA, followed by the introduction of the Alexa Fluor® 488 Phalloidin for 20 min. The cells were stained with 4′,6-diamidino-2-phenylindole (DAPI) for 4 min and washed three times with PBS. Images were obtained using a Leica TCS SP8 confocal microscope. The confocal microscopy settings were kept the same between the samples and were acquired with a 400× optical zoom.

2.5 3D assays

2.5.1 3D culture. The cell culture 3D assays were performed using the "on top" culture method based on the procedure of Lee et al.[27] For this, 48-well plates were coated with a thin layer of a laminin-rich extracellular matrix (lrECM): Matrigel® and incubated for 20 min at 37 °C and 5% CO$_2$. Then, the A549 and MRC-5 cells were seeded, and the plates were kept in an incubator for 15 min. Next, a solution of a medium containing 10% Matrigel® was deposited onto the cells. The multicellular structures were formed after 4 days.

2.5.2 Morphology assay. The cells (2.5×10^4 per 100 μL) were cultured in sterile 48-well plates, and after the formation of multicellular structures (4 days), the treatment was performed with 4 μM of RuNO$_2$TPyP for 24 h. Next, the structures were irradiated with a dose of 4 J cm^{-2} at 415 nm and incubated under same conditions. Images were captured 24, 48, and 72 h after irradiation using a Nikon Eclipse Ti microscope.

2.5.3 Live/dead assay. Calcein acetoxymethyl-diacetylester (calcein AM) and PI were used to determine the cytotoxicity. The cells (2.5×10^4 per 100 μL) were cultured in sterile 48-well plates, and after the formation of multicellular structures (4 days), the cells were treated with 4 μM of RuNO$_2$TPyP for 24 h. Next, the medium was removed, and a fresh medium without phenol red was added. Next, the structures were irradiated with 4 J cm^{-2} at 415 nm and incubated again under same conditions. After 72 h, the multicellular structures were stained with calcein AM (1 μg mL^{-1}) and PI (5 μM mL^{-1}) for 1 h inside an incubator (37 °C, 5% CO$_2$). Then, the cells were examined with a fluorescence microscope (Nikon Eclipse Ti), and images were acquired with an optical zoom of 100×.

2.5.4 Immunofluorescence assay. For the immunofluorescence assay, the treatment was performed with 2 μM of RuNO$_2$TPyP for 24 h after the formation of the multicellular structures. The medium was then removed, and a fresh medium without phenol red was added. Next, the structures were irradiated with 4 J cm^{-2} at 415 nm and incubated again under same conditions for 24 h. Next, the structures were removed from the wells and placed on the slides. They were then fixed with a 4% paraformaldehyde solution and washed three times with 50 mM PBS glycine. Later, the slides were blocked in an immunofluorescence solution with BSA and fragments of goat anti-mouse IgG F(ab1)$_2$ antibodies. The labeling was then performed using the primary anti-caspase-3 antibody, followed by the addition of Alexa Fluor-488 second-

ary antibodies. The nuclei were stained with 0.5 μg mL^{-1} of DAPI. The slides were photographed with a Leica TCS SP8 confocal microscope. The confocal microscopy settings were kept the same between the samples and acquired with an optical zoom of 400×.

2.6 Statistical analysis

All statistical analyses were performed using the GraphPad® Prism version 8.0 software. The differences between the groups were assessed using a one-way analysis of variance (ANOVA), followed by Tukey's *post hoc* test, and considered significant at the $p < 0.05$ level. All the assays were executed at least in triplicate, and all the figures presented are representative of one of the three triplicates.

3   Results and discussion

The synergistic interaction between NO and ROS in targeting cancer cells has been demonstrated for certain ruthenium complexes upon exposure to visible light irradiation.[28,29] In the context of the RuNO$_2$TPyP complex, the NO production can arise from oxygen transfer reactions and/or photochemical processes, as previously described for species of the type [RuL$_5$(NO$_2$)(κ-N)].[30–32] Simultaneously, the absorption of photons triggers electronic excitation, enabling energy transfer to the molecular oxygen present in the medium and consequently the production of singlet oxygen.[33,34] This process, commonly termed as Type II reaction, has extensive applications in various fields, notably in PDT, where the selective production of a singlet oxygen can induce photocytotoxicity in cancer cells.[35,36]

The results from the evaluation of the cytotoxicity and photocytotoxicity effect of the complex RuNO$_2$TPyP towards tumor lung cells (A549) and non-tumor lung cells (MRC-5) reveal that the complex presents high photocytotoxicity after light irradiation in a concentration and time-dependent manner in both cell lines. IC$_{50}$ values for complex RuNO$_2$TPyP are 0.59 and 0.15 μM for the A549 cells after 4 and 24 h incubation (Fig. 2A and B), respectively, and 0.53 and 0.16 μM for the MRC-5 cells after 4 and 24 h incubation, respectively, (Fig. S2, see ESI†). Conversely, our findings indicate that in the dark, the complex did not result in cytotoxicity (<10%) at the highest concentration tested (50 μM). Despite the absence of selectivity among the cell lines in the presence of light, this complex shows significant potential as a PS, as it exhibits a low cytotoxicity in the dark. This allows for the valuable application of PDT in precisely delivering light to the targeted region during the treatment,[37] inducing only photocytotoxicity. Due to physicochemical characteristics, there was no complex aggregation observed at any of the concentrations used in the study.[24]

Interesting results emerged from cytotoxicity assays when considering the relationship between cellular uptake and incubation duration. These factors were investigated in lung cancer cells following incubation periods with RuNO$_2$TPyP of 4 and
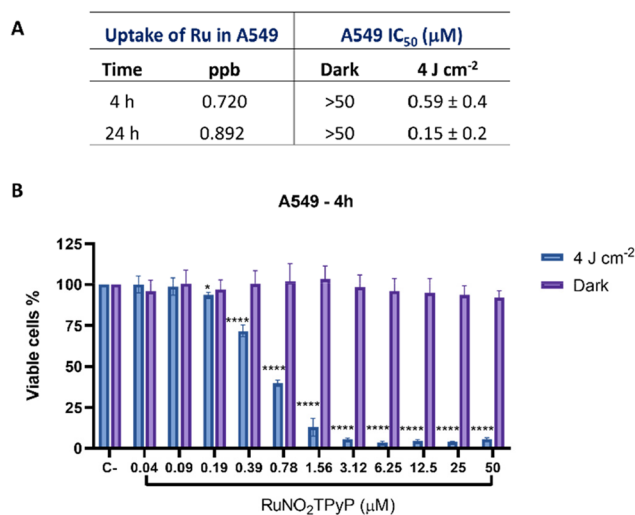

Fig. 2 Effects of RuNO$_2$TPyP on the A549 cells. (A) Ruthenium concentration (ppb) in the A549 cells after 4 or 24 h incubation with RuNO$_2$TPyP, and IC$_{50}$ (μM) of the A549 cell line after 4 and 24 h treatment. (B) Percentage of viable A549 cells after 4 h treatment with the RuNO$_2$TPyP complex in the presence of irradiation (415 nm, dose 4 J cm^{-2}, represented in light blue) and absence of irradiation (dark, represented by light purple). Percentage results were compared with the negative control (C-), (*$p < 0.05$, **$p < 0.01$, ***$p < 0.001$ and ****$p < 0.0001$).

24 h, ICP-MS analysis was utilized for quantifying the ruthenium content. The uptake experiment revealed a time-dependent trend, exhibiting an approximate 20% rise in ruthenium concentration after extending the incubation time by 20 h. Notably, final concentration of the ruthenium complex was within the picomolar range (approximately 0.3×10^{-12} M), indicating potent cytotoxicity against the lung cancer cell line (A549) (Fig. 2A).

A cellular morphology assay was performed to further investigate the cytotoxicity analysis. Changes in cell morphology of both cell lines related to the cytotoxicity of the complex can be observed, such as a decrease in the number of the cells and the appearance of circular structures (Fig. 3A). To highlight the cells with the most different morphology, arrows are used to indicate them. To better assess the cytotoxic and cytostatic potential of the complex, we conducted a colony formation assay, which has a longer incubation time (10 d) after treatment, followed by light irradiation. This allowed us to assess the long-term effects of the complex on the growth capacity of the tumor cells, providing a comprehensive evaluation of cell response over time. Notably, the incubation with the complex was more effective in reducing the number and area of tumor cell colonies than the non-tumor cells (Fig. 3B–D).

A wound-healing assay was performed (Fig. 4A and B) to investigate the potential anti-migratory effects of the complex. This assay is important in evaluating new cancer drugs as it assesses the ability of a compound to inhibit cell migration, a key feature of tumor metastasis.[38] After 4 h of treatment with RuNO$_2$TPyP (0.06 μM) followed by irradiation, the migration of
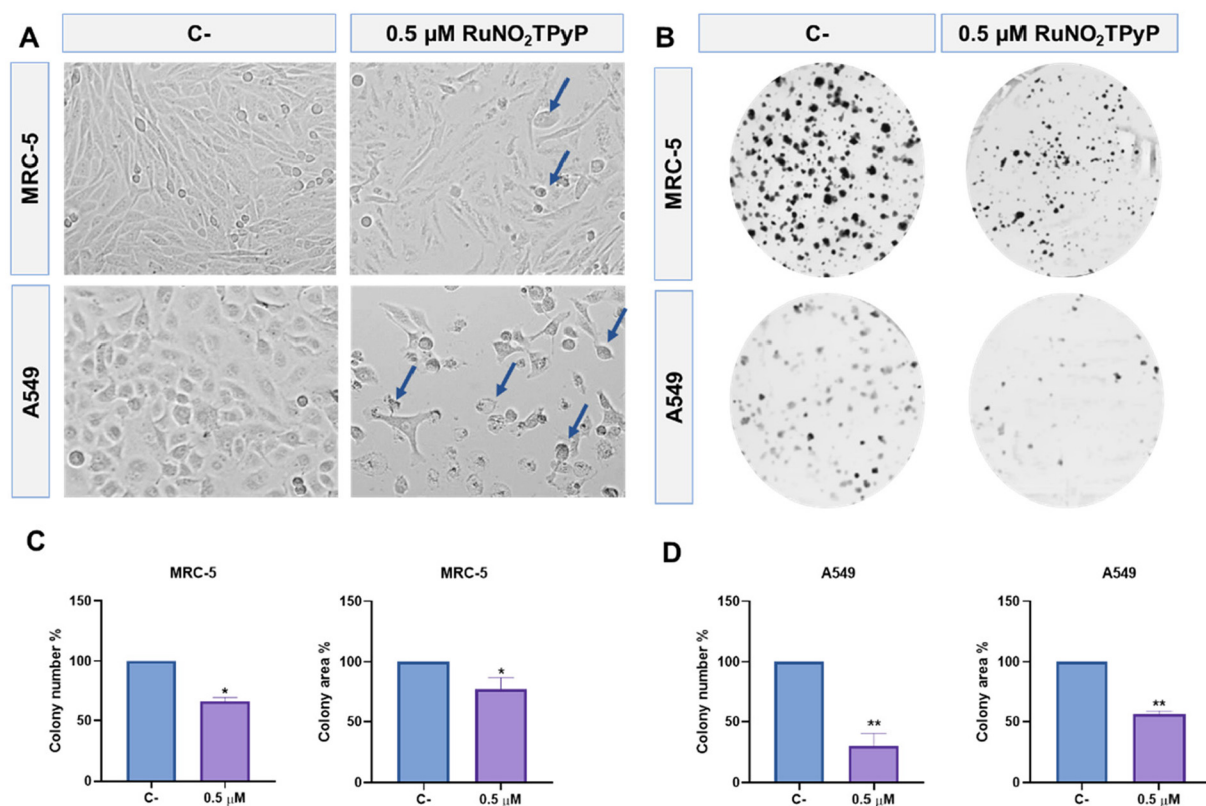
Fig. 3 Effects of RuNO$_2$TPyP on MRC-5 and A549 after 4 h of treatment (0.5 μM) followed by irradiation at 415 nm (4 J cm^{-2}) on (A) cell morphology, arrows indicate drastic alterations in morphology; (B) colony formation; and (C) quantitative analysis of MRC-5 colony numbers and area (D) quantitative analysis of A549 colony number and area (*p < 0.05 and **p < 0.01).

the A549 lung tumor cells was significantly inhibited from 24 h onwards. In contrast, the complex did not inhibit the migration of the MRC-5 non-tumor lung cells at 24 and 48 h, as observed in graphs depicting wound closure percentages (Fig. 4B). The light blue line represents untreated cells, while the light purple line represents treated cells, thus, illustrating the more specific activity of the complex in inhibiting the migration of the tumor cells.

Exposing cells to cytotoxic agents can lead to changes in their cytoskeleton, a complex protein network responsible for cell shape and motility, among other functions.[39] To evaluate the effects on the cytoskeleton organization after treatment with RuNO$_2$TPyP and irradiation, the cytoskeleton staining assay was performed using Alexa 488 Fluor® Phalloidin as a marker for F-actin fibers. The complex induced changes in the cytoskeletons of the A549 and MRC-5 cells at the concentrations tested. However, more significant alterations were found in the tumor cell line compared to the non-tumor cell line (Fig. 4C).

The cell cycle assay was used to evaluate the ability of the complex to alter the cell cycle distribution and to induce fragmentation. The results (Fig. 5A) demonstrate that changes in the cell cycle are similar in the A549 and MRC-5 cells. The complex induces an increase in the cells in the sub-G1 phase, which is indicative of nuclear fragmentation, in a concen-

tration-dependent manner when compared to the negative control. In the other cycle phases, the complex decreases cells when compared to the control.

Therefore, based on previous results, we chose to perform the apoptosis assay, because the DNA fragmentation is a hallmark of apoptosis[40] and changes in actin filaments are a significant characteristic of the apoptotic process.[41] RuNO$_2$TPyP induced apoptosis in the A549 and MRC-5 cells. In the A549 cells, at 2 μM of RuNO$_2$TPyP, the percentage of the tumor cells in apoptosis is approximately 56%. In the non-tumor cells, the percentage of the cells in apoptosis is approximately 45%, demonstrating that the complex is somewhat more specific in inducing apoptosis in the tumor cells (Fig. 5B and C). In another study, anionic porphyrin (1-Zn) demonstrated its ability to induce apoptosis in the A549 cells at a concentration of 16 μM, particularly in conjunction with irradiation. This was supported by a substantial increase in the sub-G0/G1 peak, which indicated DNA fragmentation and the observation that more than 40% of the cells were in the late apoptosis phase after treatment and irradiation.[42]

The interaction of ruthenium complexes with transport biomolecules has already been described in the literature.[43] To evaluate this interaction, we performed an assay with the A549 cells that combined a fixed 0.25 μM concentration of RuNO$_2$TPyP with different concentrations of BSA and apo-Tf.

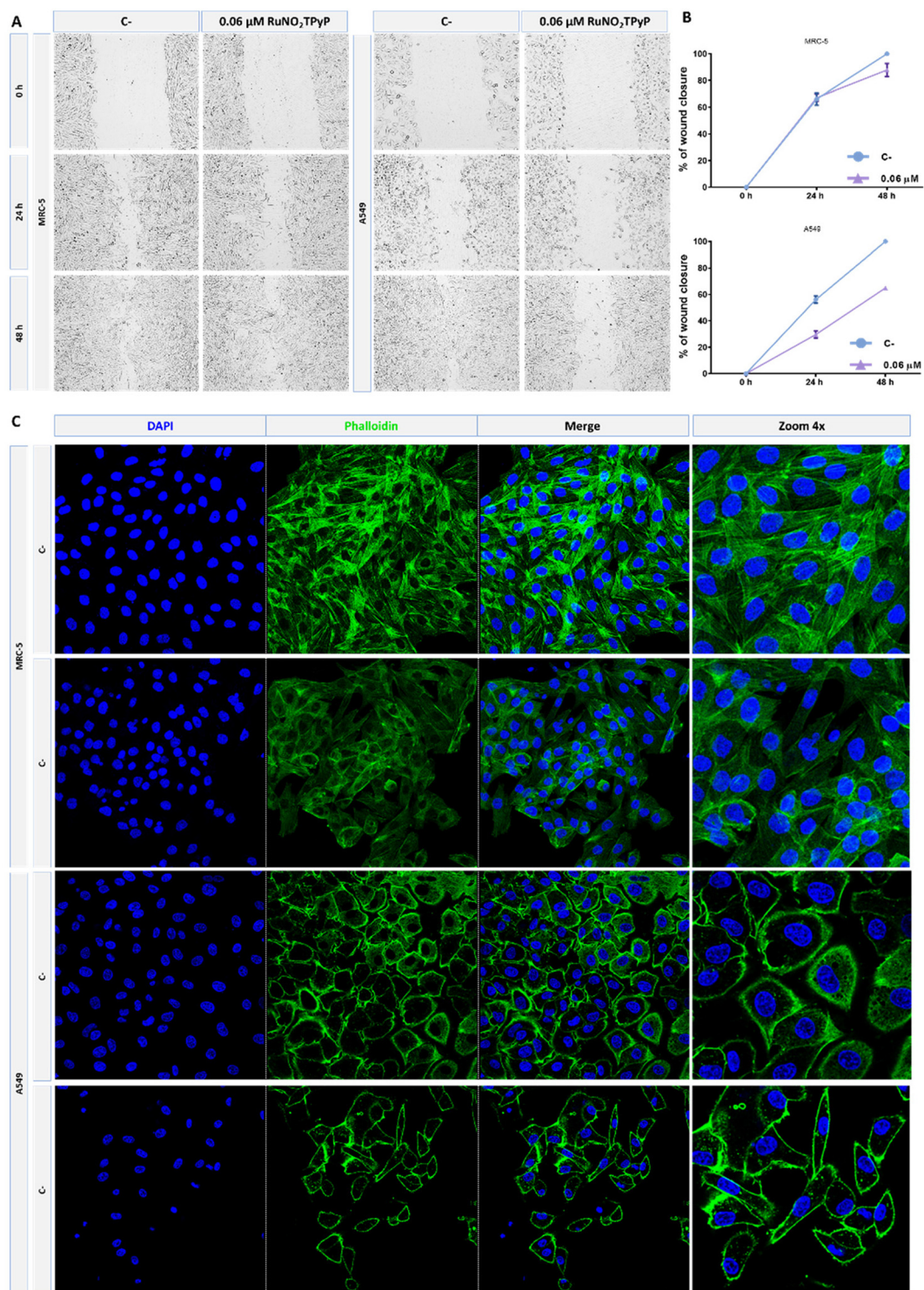**Fig. 4** Effects of RuNO$_2$TPyP after 4 h of treatment followed by irradiation at 415 nm (dose 4 J cm^{-2}) on the MRC-5 and A549 cell migration and cytoskeleton. (A) Wound healing assay in the A549 and MRC-5 cells at 0, 24, and 48 h after irradiation; (B) percentage of wound closure of the A549 and MRC-5 treated cells (light purple) compared to untreated cells (C−) (light blue); (C) cytoskeleton staining assay with phalloidin and DAPI. The negative control (C−) corresponds to the untreated cells.

Fig. 6 shows that the highest concentrations of BSA and apo-Tf tested can significantly interact with the complex, increasing its cytotoxicity. Therefore, we can infer that part of the internalization of the complex into the cells occurs by biomolecular transport entities present in the biological environment.
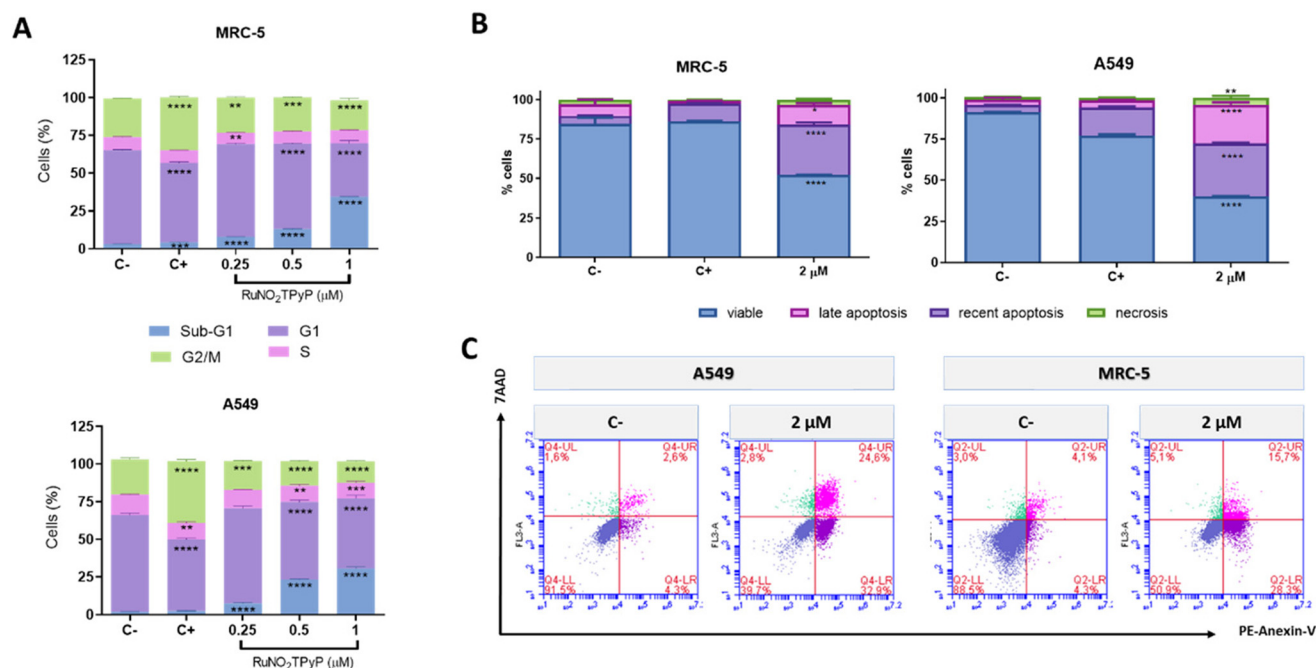
Fig. 5 Effects of RuNO$_2$TPyP after 4 h treatment followed by irradiation at 415 nm (dose 4 J cm^{-2}) on the MRC-5 and A549 cells cycle and apoptosis. (A) Cell cycle assay; (B) percentages of viable cells, early apoptosis, late apoptosis, and necrosis; (C) apoptosis assay with PE-Annexin V (FL2-A) and 7AAD (FL3-A). The results were compared to the negative control (C−) (no treatment) and positive control (C+) corresponding to the cells treated with 100 μM cisplatin (* $p \leq 0.05$, ** $p \leq 0.01$, and *** $p \leq 0.001$).
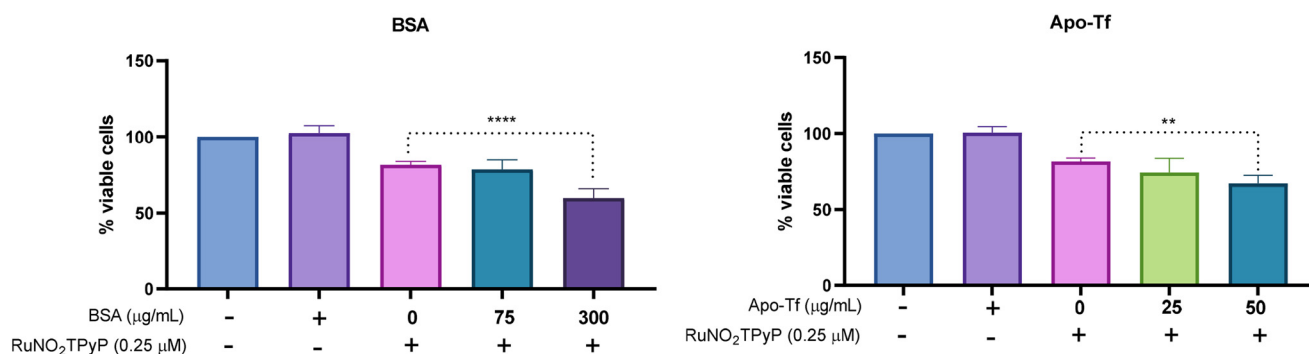
Fig. 6 Interaction of RuNO$_2$TPyP with BSA and apo-Tf in A549 cells. The cells were incubated with 0.25 μM of the complex and different concentrations of BSA and apo-Tf for 4 h in the presence of irradiation at 415 nm (4 J cm^{-2}). The results were compared to the groups of cells treated only with the complex, without BSA or apo-Tf (** $p < 0.01$ and ****$p < 0.0001$).

To evaluate NO production after 4 h of treatment with RuNO$_2$TPyP followed by irradiation and another 20 h of incubation, the A549 and MRC-5 cells were labeled with the fluorescent probe DAF-FM and examined under a fluorescence microscope. This probe is cell-permeable and is used for NO detection. The results shown in Fig. 7A demonstrate that the complex induces NO formation in the cells upon irradiation. It should be noted that the images were obtained 20 h after irradiation, and NO appears in cells that underwent a change in morphology.

Treatment with RuNO$_2$TPyP at 1 μM resulted in an immediate increase in cellular ROS production following irradiation,

as evidenced by the DCFH-DA assay. It is important to note that this reagent, while useful in evaluating oxidative stress, captures a spectrum of reactive oxygen species and is not specific to singlet oxygen.[44] To specifically confirm singlet oxygen generation, photochemical assays were carried out in our previously study.[24] These assays provided direct measurements of singlet oxygen production by its phosphorescence at 1270 nm leading us to calculate the quantum yield for the complex ($\Phi_\Delta = 0.29$) based on TPP ($\Phi_\Delta = 0.52$), thereby confirming the accuracy of our assertion and supporting findings observed in the fluorescence assay. A comparison of fluorescence levels between the complex and hydrogen peroxide
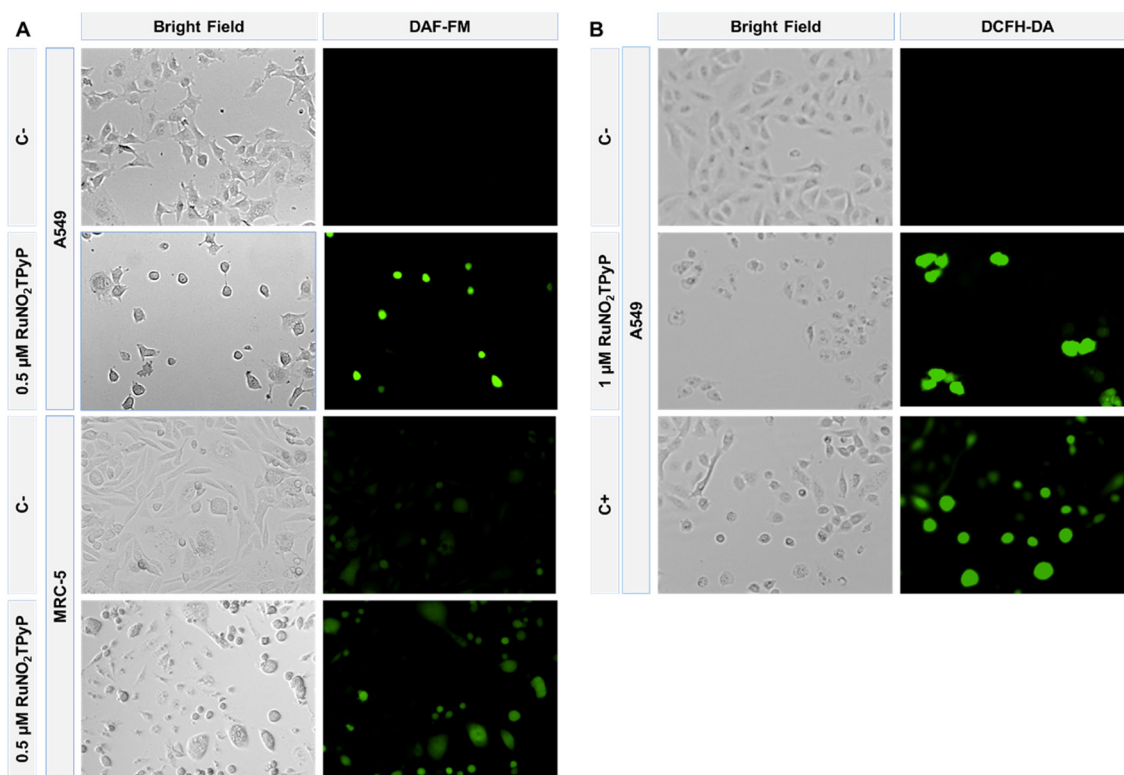
Fig. 7 Evaluation of NO and ROS intracellular production after 4 h treatment with RuNO$_2$TPyP (0.5 μM) followed by irradiation at 415 nm (4 J cm^{-2}). (A) Intracellular NO production was detected using the DAF-FM reagent, and fluorescence microscopy images were captured 20 hours after irradiation; (B) general ROS production was evaluated using DCFH-DA, with hydrogen peroxide (10 000 μM) acting as the positive control (C+). The negative control (C−) consists of untreated cells.

(positive control) with the untreated cells (negative control) (Fig. 7B) indicates that all treatments induce ROS formation. However, the complex does so at a significantly lower concentration. Such an ability is highly advantageous for further investigations and potential applications of the complex as a PS. Another study showed that the new PSs, chlorin-e$_6$ 13^1-guanidinoethylcarboxamide and chlorin-e6 13^1-boc$_2$guanidinoethylcarboxamide exhibited higher phototoxicity. Incubating cells with 1 μM of these compounds for 4 h led to enhanced photogeneration of ROS.[45] The observed outcomes align with the expected results of PDT, as the generation of ROS is a critical mechanism in this process.[46]

The common testing models for new compounds use two-dimensional (2D) cell cultures. Despite the undeniable contributions of these models, they present limitations that result in a low success rate of drugs in the discovery process and, consequently, low efficiency of the investment made.[47] A 3D culture has attractive advantages over 2D models, because it allows cell–cell and cell–extracellular matrix (ECM) interactions.[48] Several studies have highlighted notable distinctions between cells cultivated using the traditional 2D and more advanced 3D matrix models. Specifically, some research indicates that cells grown in 2D exhibit a higher sensitivity to cytotoxic drugs compared to those cultured in 3D. For example, a recent study found noticeable differences in the cytotoxicity of epirubicin,

cisplatin, and docetaxel with 13 triple-negative breast cancer cell lines between 2D and 3D (spheroid) cultures. In most cell lines, the IC$_{50}$ values for all three drugs were significantly higher in the 3D cultures when compared to their 2D counterparts.[49] These findings underscore the significance of employing these newer models for testing purposes.[50,51]

Given the interesting results of RuNO$_2$TPyP using 2D cell cultures, it is relevant to advance studies using 3D cell cultures. The first 3D assay with RuNO$_2$TPyP was the morphology assay, which aimed to verify whether, under 3D conditions, the complex can induce morphological changes in the multicellular structures. Fig. 8A demonstrates that the complex modified the morphology of the 3D multicellular structures, mainly those formed by the A549 cells, which exhibited fragmentation.

A cytotoxicity assay was conducted using double staining with calcein-AM and PI to assess the cytotoxicity of the complex in the 3D multicellular structures formed by the A549 cells. The results (Fig. 8B) revealed that after 24 h of treatment followed by irradiation and an additional 72 h of incubation, the intensity of the red staining in the multicellular structures increased significantly, indicating cell death. In contrast, the control group displayed intact structures with prominent green staining. Based on the analysis of different multicellular structures, it can be observed that there was a reduction in the size
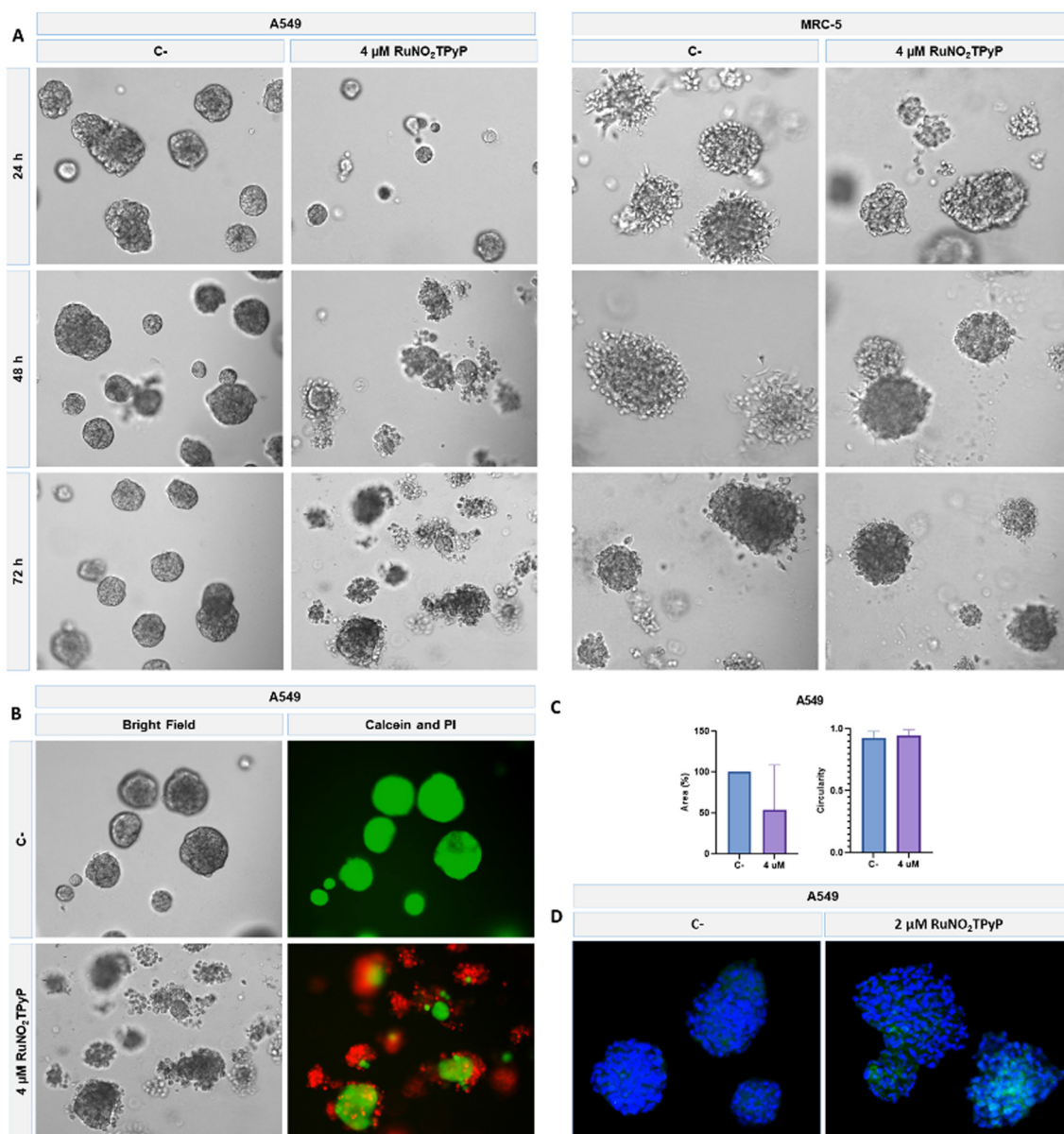
Fig. 8 Effects of RuNO$_2$TPyP on 3D cell culture after 24 h of treatment followed by irradiation at 415 nm (4 J cm^{-2} dose). (A) Effects of the complex on the morphology of the MRC-5 and A549 multicellular structures after 24, 48, and 72 h of irradiation; (B) cytotoxic effects of the complex after 72 h of irradiation on the A549 multicellular structures. Calcein-AM is shown in green and PI in red; (C) area and circularity of the multicellular structures formed in 3D by the A549 cells after 72 h of irradiation; (D) effects of the complex on apoptosis in 3D. The multicellular structures formed by the A549 cells were stained with anti-caspase-3 24 h after irradiation. This figure is composed of randomly selected multicellular structures. The nuclei were stained with DAPI (blue), while activated caspase-3 staining is shown in green.

of these structures. Nevertheless, there was no alteration in their circularity (Fig. 8C). Circularity can indicate the malignancy and aggressiveness of the tumor, as more circular structures are less likely to be tumors.[52] To investigate the potential activation of apoptosis by the complex in 3D and 2D cultures, an immunostaining assay utilizing a cleaved anti-caspase-3 antibody was performed. Fig. 8D illustrates positive staining for cleaved caspase-3 (in green), particularly at the center of the multicellular structures at a concentration of 2 μM, reinforcing results obtained in 2D experiments.

4 Conclusions

The present study investigated the effects of the nitro-ruthenium porphyrin complex, RuNO$_2$TPyP, in lung cells (MRC-5 and A549) using 2D and 3D cell culture models. Our findings demonstrated that despite its limited cellular uptake, this complex exhibited remarkable photocytotoxicity against lung cells while maintaining low cytotoxicity. Treatment of cells with low concentrations of RuNO$_2$TPyP followed by light irradiation at a dose of 4 J cm^{-2} at 415 nm induced profound

changes in cell morphology, presented cytostatic effects, inhibited cell migration, disrupted the cellular cytoskeleton, altered the cell cycle, triggered apoptosis, and stimulated the intracellular generation of NO and ROS. As anticipated, the performance of the complex did not exhibit significant variation among the cell lines because PDT involving ROS aims at local treatment rather than compound selectivity. However, data shows that the complex was more photocytotoxic to the tumor cell line. In the 3D cell culture model, $RuNO_2TPyP$ induced changes in the morphology of multicellular structures formed by the A549 cells. It also exhibited significant photocytotoxicity and induced apoptosis in the tumor cell structures, highlighting its potential therapeutic efficacy in a more physiologically relevant setting than 2D cell assays. Overall, our results indicate that $RuNO_2TPyP$ shows significant potential as a PS for lung cancer treatment. These effects are attributed to the release of NO and generation of singlet oxygen during light irradiation, suggesting a possible synergistic mechanism. Further studies are necessary to fully elucidate complete potential and mechanisms of action of this complex.

Abbreviations

2D	Two-dimensional
3D	Three-dimensional
7AAD	7-Aminoactinomycin D
DCFH-DA	Dichlorodihydrofluorescein diacetate
DMEM	Dulbecco's modified Eagle's medium
DMSO	Dimethyl sulfoxide
ECM	Extracellular matrix
FBS	Fetal bovine serum
IC_{50}	Half-maximal inhibitory concentration
ICP-MS	Inductively coupled plasma mass spectrometry
lrECM	Laminin-rich extracellular matrix
MTT	[3-(4,5-Dimethylthiozol-2-yl)-2,5-diphenyltetrazolium bromide]
PDT	Photodynamic therapy
PI	Propidium iodide
PS	Photosensitizer
PE	Phycoerythrin
PPB	Parts per billion
ROS	Reactive oxygen species

Data availability

The datasets generated during the current study are available upon reasonable request from the corresponding author.

Conflicts of interest

The authors declare that they have no conflicts of interest.

Acknowledgements

References

1 D. Sun, W. Gao, H. Hu and S. Zhou, *Acta Pharm. Sin. B*, 2022, **12**, 3049–3062.

2 V. Oliveri, *Front. Mol. Biosci.*, 2022, **9**, 841814.

3 L. Falzone, S. Salomone and M. Libra, *Front. Pharmacol.*, 2018, **9**, 1300.

4 L. Zhong, Y. Li, L. Xiong, W. Wang, M. Wu, T. Yuan, W. Yang, C. Tian, Z. Miao, T. Wang and S. Yang, *Signal Transduction Targeted Ther.*, 2021, **6**, 201.

5 N. Hammoudi, K. B. Riaz Ahmed, C. Garcia-Prieto and P. Huang, *Chin. J. Cancer*, 2011, **30**, 508–525.

6 M. G. Vander Heiden and R. J. DeBerardinis, *Cell*, 2017, **168**, 657–669.

7 Z. J. Li and C. H. Cho, *Eur. J. Pharmacol.*, 2011, **667**, 17–22.

8 F. Vannini, K. Kashfi and N. Nath, *Redox Biol.*, 2015, **6**, 334–343.

9 L. A. Ridnour, D. D. Thomas, C. Switzer, W. Flores-Santana, J. S. Isenberg, S. Ambs, D. D. Roberts and D. A. Wink, *Nitric Oxide*, 2008, **19**, 73–76.

10 A. C. Pereira, M. Paulo, A. V. Araújo, G. J. Rodrigues and L. M. Bendhack, *Braz. J. Med. Biol. Res.*, 2011, **44**, 947–957.

11 C. N. Lunardi, R. S. da Silva and L. M. Bendhack, *Braz. J. Med. Biol. Res.*, 2009, **42**, 87–93.

12 C. Z. Ferezin, F. S. Oliveira, R. S. da Silva, A. R. Simioni, A. C. Tedesco and L. M. Bendhack, *Nitric Oxide*, 2005, **13**, 170–175.

13 T. Mishchenko, I. Balalaeva, A. Gorokhova, M. Vedunova and D. V. Krysko, *Cell Death Dis.*, 2022, **13**, 455.

14 P. Agostinis, K. Berg, K. A. Cengel, T. H. Foster, A. W. Girotti, S. O. Gollnick, S. M. Hahn, M. R. Hamblin, A. Juzeniene, D. Kessel, M. Korbelik, J. Moan, P. Mroz, D. Nowis, J. Piette, B. C. Wilson and J. Golab, *CA Cancer J. Clin.*, 2011, **61**, 250–281.

15 S. Kwiatkowski, B. Knap, D. Przystupski, J. Saczko, E. Kędzierska, K. Knap-Czop, J. Kotlińska, O. Michel,

K. Kotowski and J. Kulbacka, *Biomed. Pharmacother.*, 2018, **106**, 1098–1107.

16 R. R. Allison, V. S. Bagnato and C. H. Sibata, *Future Oncol.*, 2010, **6**, 929–940.

17 C. Mari, V. Pierroz, S. Ferrari and G. Gasser, *Chem. Sci.*, 2015, **6**, 2660–2686.

18 M. Imran, M. Ramzan, A. Qureshi, M. Khan and M. Tariq, *Biosensors*, 2018, **8**, 95.

19 T. Sekrafi, Z. Denden, F. Tudorache, S. Tascu, H. Nasri and C. Dridi, *IEEE International Conference on Design & Test of Integrated Micro & Nano-Systems (DTS)*, 2019, 1–5.

20 C. Imberti, P. Zhang, H. Huang and P. J. Sadler, *Angew. Chem., Int. Ed.*, 2020, **59**, 61–73.

21 O. Mazor, A. Brandis, V. Plaks, E. Neumark, V. Rosenbach-Belkin, Y. Salomon and A. Scherz, *Photochem. Photobiol.*, 2007, **81**, 342–351.

22 S. Mallidi, A. P. Khan, H. Liu, L. Daly, G. Rudd, P. Leon, S. Khan, B. M. A. Hussain, S. A. Hasan, S. A. Siddique, K. Akhtar, M. August, M. Troulis, F. Cuckov, J. P. Celli and T. Hasan, *Sci. Rep.*, 2019, **9**, 1–8.

23 G. Ghosh, K. L. Colón, A. Fuller, T. Sainuddin, E. Bradner, J. McCain, S. M. A. Monro, H. Yin, M. W. Hetu, C. G. Cameron and S. A. McFarland, *Inorg. Chem.*, 2018, **57**, 7694–7712.

24 M. T. Martin, A. B. Becceneri, P. C. Ford and R. S. da Silva, *Inorg. Chem. Commun.*, 2024, **161**, 112138.

25 T. Mosmann, *J. Immunol. Methods*, 1983, **65**, 55–63.

26 P. Y. K. Yue, E. P. Y. Leung, N. K. Mak and R. N. S. Wong, *J. Biomol. Screening*, 2010, **15**, 427–433.

27 G. Y. Lee, P. A. Kenny, E. H. Lee and M. J. Bissell, *Nat. Methods*, 2007, **4**, 359–365.

28 L. C. B. Ramos, M. S. P. Marchesi, D. Callejon, M. D. Baruffi, C. N. Lunardi, L. D. Slep, L. M. Bendhack and R. S. da Silva, *Eur. J. Inorg. Chem.*, 2016, **2016**, 3592–3597.

29 Z. A. Carneiro, J. C. B. De Moraes, F. P. Rodrigues, R. G. De Lima, C. Curti, Z. N. Da Rocha, M. Paulo, L. M. Bendhack, A. C. Tedesco, A. L. B. Formiga and R. S. Da Silva, *J. Inorg. Biochem.*, 2011, **105**, 1035–1043.

30 G. Liang, M. Zhang and C. E. Webster, *Inorganics*, 2022, **10**(6), 69.

31 Kulbir, S. Das, T. Devi, M. Goswami, M. Yenuganti, P. Bhardwaj, S. Ghosh, S. Chandra Sahoo and P. Kumar, *Chem. Sci.*, 2021, **12**, 10605–10612.

32 A. M. Silva, L. B. Negri, J. C. Biazzotto, S. de Paula Machado, J. D. Santos, J. F. N. Batista, P. I. S. Maia, V. M. Deflon, L. M. Bendhack, M. R. Hamblin and R. S. da Silva, *J. Inorg. Biochem.*, 2023, **243**, 112166.

33 X. Zhang, M. C. Wasson, M. Shayan, E. K. Berdichevsky, J. Ricardo-Noordberg, Z. Singh, E. K. Papazyan, A. J. Castro, P. Marino, Z. Ajoyan, Z. Chen, T. Islamoglu, A. J. Howarth, Y. Liu, M. B. Majewski, M. J. Katz, J. E. Mondloch and O. K. Farha, *Coord. Chem. Rev.*, 2021, **429**, 213615.

34 S. K. Pushpan, S. Venkatraman, V. G. Anand, J. Sankar, H. Rath and T. K. Chandrashekar, *J. Chem. Sci.*, 2002, **114**, 311–338.

35 A. R. Sekhar, Y. Chitose, J. Janoš, S. I. Dangoor, A. Ramundo, R. Satchi-Fainaro, P. Slavíček, P. Klán and R. Weinstain, *Nat. Commun.*, 2022, **13**, 3614.

36 J. Malone, S. Klaine, C. Alcantar, F. Bratcher and R. Zhang, *New J. Chem.*, 2021, **45**, 4977–4985.

37 J. H. Correia, J. A. Rodrigues, S. Pimenta, T. Dong and Z. Yang, *Pharmaceutics*, 2021, **13**, 1332.

38 J. Pijuan, C. Barceló, D. F. Moreno, O. Maiques, P. Sisó, R. M. Marti, A. Macià and A. Panosa, *Front. Cell Dev. Biol.*, 2019, **7**, 1–16.

39 C. Ruggiero and E. Lalli, *Cancer Metastasis Rev.*, 2021, **40**, 89–140.

40 J. H. Zhang and M. Xu, *Cell Res.*, 2000, **10**, 205–211.

41 M. Desouza, P. W. Gunning and J. R. Stehn, *Bioarchitecture*, 2012, **2**, 75–87.

42 Z. Zhang, H. Yu, S. Wu, H. Huang, L. Si, H. Liu and L. Shi, *Bioorg. Med. Chem.*, 2019, **27**, 2598–2608.

43 M. A. Naves, A. E. Graminha, L. C. Vegas, L. Luna-Dulcey, J. Honorato, A. C. S. Menezes, A. A. Batista and M. R. Cominetti, *Mol. Pharm.*, 2019, **16**, 1167–1183.

44 S. H. Doak, S. M. Griffiths, B. Manshian, N. Singh, P. M. Williams, A. P. Brown and G. J. S. Jenkins, *Mutagenesis*, 2009, **24**, 285–293.

45 Y. H. Gao, V. Lovreković, A. Kussayeva, D. Y. Chen, D. Margetić and Z. L. Chen, *Eur. J. Med. Chem.*, 2019, **177**, 144–152.

46 J. M. Dąbrowski, *Adv. Inorg. Chem.*, 2017, **40**, 343–394.

47 V. Brancato, J. M. Oliveira, V. M. Correlo, R. L. Reis and S. C. Kundu, *Biomaterials*, 2020, **232**, 119744.

48 O. Habanjar, M. Diab-Assaf, F. Caldefie-Chezet and L. Delort, *Int. J. Mol. Sci.*, 2021, **22**, 12200.

49 M. Muguruma, S. Teraoka, K. Miyahara, A. Ueda, M. Asaoka, M. Okazaki, T. Kawate, M. Kuroda, Y. Miyagi and T. Ishikawa, *Biochem. Biophys. Res. Commun.*, 2020, **533**, 268–274.

50 M. Huang, J. J. Lu and J. Ding, *Nat. Prod. Bioprospect.*, 2021, **11**, 5–13.

51 F. Salehi, H. Behboudi, G. Kavoosi and S. K. Ardestani, *Sci. Rep.*, 2017, **7**, 2553.

52 A. I. Baba and C. Câtoi, *Comparative Oncology*, The Publishing House of the Romanian Academy, Bucharest (RO), 2007.